Spin correlation in the frustrated antiferromagnet MnS_2 above the Néel temperature

T. Chattopadhyay
Centre d'Etudes Nucléaires, 85X, 38041 Grenoble CEDEX, France
and Institut Laue-Langevin, 156X, 38042 Grenoble CEDEX, France

Th. Brückel
Institut Laue-Langevin, 156X, 38042 Grenoble CEDEX, France

P. Burlet
Centre d'Etudes Nucléaires, 85X, 38041 Grenoble CEDEX, France
(Received 26 December 1990; revised manuscript received 24 June 1991)

Spin correlations in the antiferromagnet MnS_2 based on an inherently frustrated face-centered-cubic lattice have been investigated by quasielastic neutron scattering above the Néel temperature. The diffuse scattering above T_N is centered at an incommensurate position $\mathbf{k}=(1,k_y,0)$ and is temperature dependent. The component k_y increases continuously from $k_y=0.40$ at $T=115$ K to $k_y=0.44$ at a temperature just above $T_N=48.2$ K. At T_N, a first-order phase transition takes place and k_y jumps abruptly to the commensurate value $k_y=\frac{1}{2}$. The ratio of the correlation lengths along and perpendicular to the incommensurate modulation is very close to unity at T_N. The spatial correlations extend only over little more than one unit cell ($\xi=8$ Å) even just above T_N. The inverse time correlation increases continuously with temperature from 0.16 THz at T_N up to 2.9 THz at 150 K, the highest temperature investigated. Mean-field calculations of the diffuse scattering in a framework of a Heisenberg Hamiltonian with exchange up to the fourth neighbors agree reasonably well with the experimental data. However, such calculations fail to explain the centering of the diffuse scattering at the incommensurate wave vector.

I. INTRODUCTION

The magnetic semiconductor MnS_2 orders with the type-III antiferromagnetic structure[1] with the wave vector $\mathbf{k}=(1,\frac{1}{2},0)$. The antiferromagnetic phase transition at $T_N=48.2$ K is found to be of first order.[2-4] According to Rossat-Mignod,[5] the type-III antiferromagnetic structure should be classified as a commensurate structure. The classical behavior in such a case would be second-order phase transition from the paramagnetic to an incommensurate phase at T_N which undergoes a lock-in transition to a commensurate phase at lower temperatures. The first-order phase transition in MnS_2 directly to the commensurate phase is unusual and its origin is an important problem to investigate. Diffuse neutron scattering above T_N gives valuable information in such cases. It samples the short-range-ordered spin fluctuations and yield broad approximate Lorentzian peaks in reciprocal (Q) space. Their positions and widths directly determine the structure and the inverse correlation lengths of the fluctuations. Diffuse neutron-scattering investigations have revealed[6,7] the origin of the first-order phase transitions in UAs and CeSb. UAs undergoes a first-order phase transition at $T_N=126$ K to the type-I antiferromagnetic structure. Above T_N the diffuse scattering was found to be anisotropic and centered about a wave vector that suggests a tendency to order with an incommensurate type-I ordering. CeSb orders at $T_N=16.4$ K in a first-order phase transition to a modulated commensurate phase.[8] Diffuse scattering above T_N shows fluctuations corresponding to the type-I phase.[9] Our preliminary studies of magnetic diffuse neutron scattering[10] in MnS_2 showed spin fluctuations centered at the incommensurate vector $\mathbf{k}=(1,0.44,0)$. We have now performed more detailed diffuse neutron-scattering investigations on MnS_2 as functions of both scattering vector Q and energy E and have determined the inverse space and time correlations as functions of temperature.

We have organized the present paper in the following way. In Sec. II we recapitulate the crystal and magnetic structure of MnS_2. The experimental procedure has been described in Sec. III. Section IV gives the results of the diffuse scattering investigations as a function of Q whereas in Sec. V we describe similar diffuse scattering investigations as a function of energy. In Sec. VI, a simple exchange model which reproduces the experimental two-dimensional diffuse scattering distribution reasonably well, is presented. Section VII is devoted to the discussion of the results and Sec. VIII gives the summary and the conclusions from the present investigations.

II. CRYSTAL AND MAGNETIC STRUCTURE OF MnS_2

The magnetic semiconductor MnS_2 crystallizes with the pyrite structure ($Pa\bar{3}$, $a_0=6.104$ Å at 295 K) which, along with the closely related marcasite and arsenopyrite structure, are exhibited by a large number of compounds with diverse electrical and magnetic properties.[11] In

these compounds the cations are sixfold coordinated by distorted octahedra of anions whereas the anions are tetrahedrally (distorted) bonded to three cations and one anion forming covalently bonded anion pairs (Fig. 1). The structure can be viewed as the rocksalt structure in which the anions are replaced by covalently bonded dumbbell-shaped anion pairs placed in between cations and directed along ⟨111⟩. The structure therefore does not retain the full symmetry of the space group $Fm3m$ of the rocksalt structure and has a lower symmetry space group $Pa\bar{3}$.

Figure 2 illustrates the type-III magnetic structure of MnS_2. The magnetic unit cell is doubled in one of the cubic ⟨100⟩ directions. The magnetic structure can be considered to consist of antiferromagnetic layers $A,B,\bar{A},\bar{B}$, where $\bar{A}$ and $\bar{B}$ are obtained by reversing the spin directions. The spins are oriented along the cubic direction for which the magnetic cell is doubled. This is a single-**k** structure and it cannot be distinguished from a double-**k** or a triple-**k** structure unless one applies uniaxial stress or external magnetic field. By applying a magnetic field parallel to [100] and [110] we have recently established that the magnetic structure of MnS_2 is actually of the single-**k** type.[12]

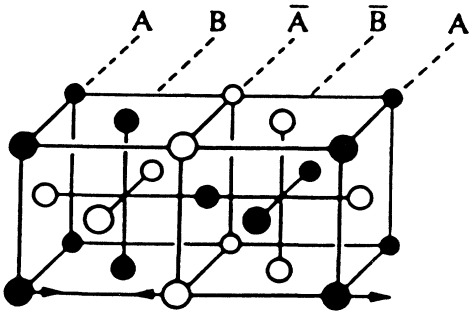

FIG. 2. Type-III single-**k** antiferromagnetic structure of MnS_2. The solid and open circles represent atoms with oppositely directly spin orientations. The sulfur atoms have been omitted.

III. EXPERIMENTAL PROCEDURES

We have used a natural single crystal of MnS_2 (hauerite) of octahedral shape with linear dimensions of about 1 cm for the present investigations. We have performed x-ray- and neutron-diffraction measurements[13] on parts of the crystal at several temperatures and the structural refinements using these data showed that the quality of the crystal is very good. Magnetic diffuse neutron-scattering investigations have been performed with the four-circle-diffractometer-cum-triple-axis spectrometer D10 situated in the guide hall of the High Flux Reactor of the Institut Laue-Langevin. The crystal was fixed to the four-circle helium-flow cryostat by aluminum foil without using any glue to reduce the background scattering. Neutrons of wavelength 2.36 Å were provided by a pyrolytic graphite monochromator (PG 002) in combination with a PG filter. During the experiment we have employed D10 in the two-axis configuration for the integral scans and in the triple-axis configuration for the inelastic scans. In the latter mode, a PG 002 analyzer was used and the collimation was typically 30′-60′-60′-40′.

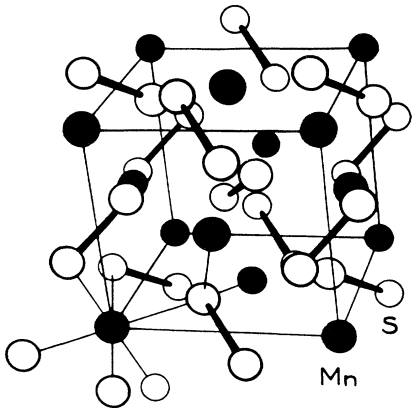

FIG. 1. Crystal structure of the pyrite-type MnS_2.

IV. MAGNETIC DIFFUSE SCATTERING AS A FUNCTION OF Q

MnS_2 undergoes a first-order phase transition from the paramagnetic phase to the type-III phase at about $T_N=48.2$ K. We have redetermined the Néel temperature by measuring the temperature dependence of the intensity of the scattered neutrons at a reciprocal point $\mathbf{Q}=(1,1.4,0)$, which is close to the magnetic Bragg reflection (1,1.5,0) in the ordered state. The integral neutron intensity at this point is proportional to the static susceptibility. Figure 3 shows the temperature dependence of the scattered neutron intensity at $\mathbf{Q}=(1,1.4,0)$. Below T_N, the neutron intensity increases slowly with increasing temperature until, at $T_N=48.2$ K, the intensity jumps by a factor of about 3.3 and then again decreases

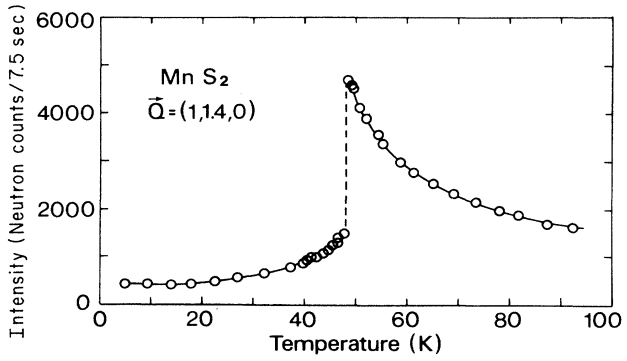

FIG. 3. Temperature variation of the intensity of the scattered neutrons from MnS_2 at $\mathbf{Q}=(1,1.4,0)$. This intensity, at a point slightly away from the magnetic Bragg peak position of the ordered phase, is proportional to the static susceptibility. The discontinuous jump in intensity at $T_N=48.2$ K corresponds to the first-order phase transition.

with increasing temperature. This behavior is typical for a first-order phase transition and is very similar to that observed, for example, in UAs by Sinha *et al.*[6] Figure 4 shows the temperature variation of the diffuse scattering in Q scans along **b*** through the magnetic superlattice point $(1,\frac{1}{2},0)$ together with a similar scan in the long-range-ordered phase. At $T=106.0$ K, a rather weak magnetic scattering contribution is observed which becomes increasingly more prominent at lower temperatures. The solid curves are the results of the least-squares fit to the experimental data with a Lorentzian function convoluted with a Gaussian resolution function. The asymmetry of the background seen in Fig. 4 is due to a neighboring maxima of the diffuse scattering. This can be seen in the two-dimensional scans presented in Sec. VI D. We have checked in detail that the assumed behavior of the background does not influence the results for the position and width of the Lorentzian up to temperatures around 70 K, well above T_N. The centroid of the diffuse scattering does not coincide with the commensurate superlattice point $(1,\frac{1}{2},0)$ but corresponds to an incommensurate position $\mathbf{k}=(1,k_y,0)$, which is weakly temperature dependent. Figure 5 shows the temperature dependence of the component k_y of this incommensurate vector. The component k_y increases continuously from $k_y=0.40$ at $T=115$ K to $k_y=0.44$ at a temperature just

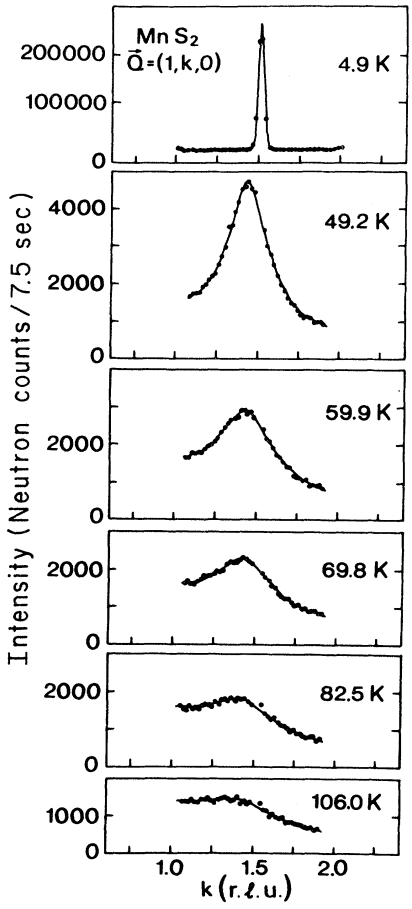

FIG. 4. Magnetic diffuse neutron scattering of MnS_2 in Q scans parallel to the modulation vector at different temperatures above T_N. The magnetic Bragg peak at a temperature below T_N is also shown for comparison. The solid curves fitted to the data are of Lorentzian form, convoluted with the Gaussian resolution function determined from a similar scan below T_N.

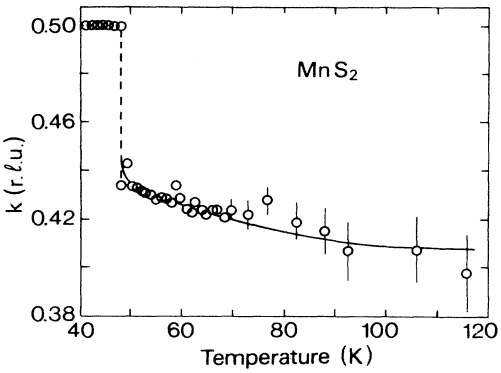

FIG. 5. Temperature variation of the incommensurate component of the vector at which the diffuse magnetic neutron scattering is centered.

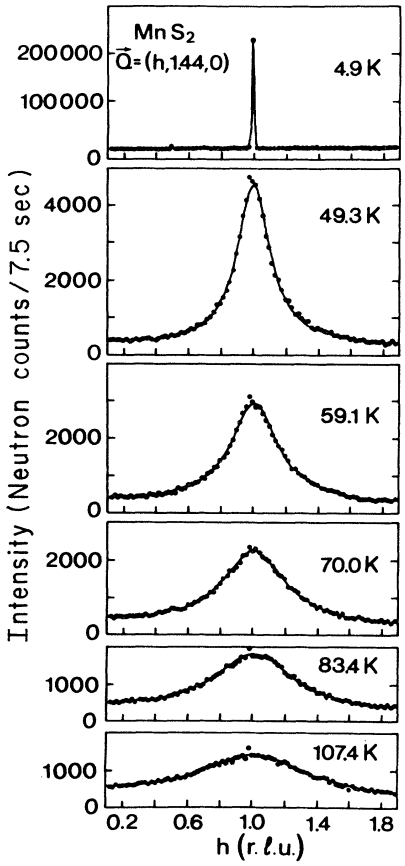

FIG. 6. Diffuse magnetic neutron scattering of MnS_2 in Q scans perpendicular to the incommensurate modulation at different temperatures. The solid curves fitted to the data are of Lorentzian form convoluted with the Gaussian resolution function.

above $T_N=48.2$ K. At T_N, k_y jumps abruptly to the commensurate value $\frac{1}{2}$. Such behavior has been observed for the first time to our knowledge in any magnetic system. Figure 6 shows the temperature dependence of the Q scans parallel to $\mathbf{a}^*$ around $\mathbf{Q}=(1,1.44,0)$. The diffuse scattering is well centered at the commensurate value $k_x=1$. Figure 7(a) shows the temperature variation of inverse correlation lengths parallel and perpendicular to the incommensurate modulation obtained from the scans of Figs. 4 and 6. The ratio of the correlation lengths parallel and perpendicular to the modulation vector is about 1 close to T_N, but it increases with temperature attaining a value of about 1.8 at $T=115$ K. Due to the uncertainty of the background, the correlation length parallel to the modulation vector obtained by the fitting procedure is uncertain. We are therefore not certain whether the anisotropy in correlation lengths at temperatures higher than about 70 K is really physical. The correlation length just above T_N is only about 8 Å along these two directions. Figure 7(b) shows the temperature variation of the peak intensity of the diffuse scattering as a function of temperature. The peak intensity is proportional to the susceptibility. The peak intensity increases as the temperature decreases and approaches T_N. Although the antiferromagnetic phase transition in MnS_2 is of first order, one can perhaps assume critical behavior of the correlations lengths at least close to the phase transition temperature. Also, in strongly frustrated systems, the critical region is known to be extended. We have fitted the correlation lengths to the three-dimensional Heisenberg critical exponent $\nu=0.7020$.

$$\kappa=\kappa_0^+ t^{\nu}, \quad T>T_c ,$$

where the reduced temperature $t=(T-T_{\text{eff}})/T_{\text{eff}}$ and T_{eff} is the effective Néel temperature. The perpendicular correlation $\kappa_\perp$ data which have been measured very accu-

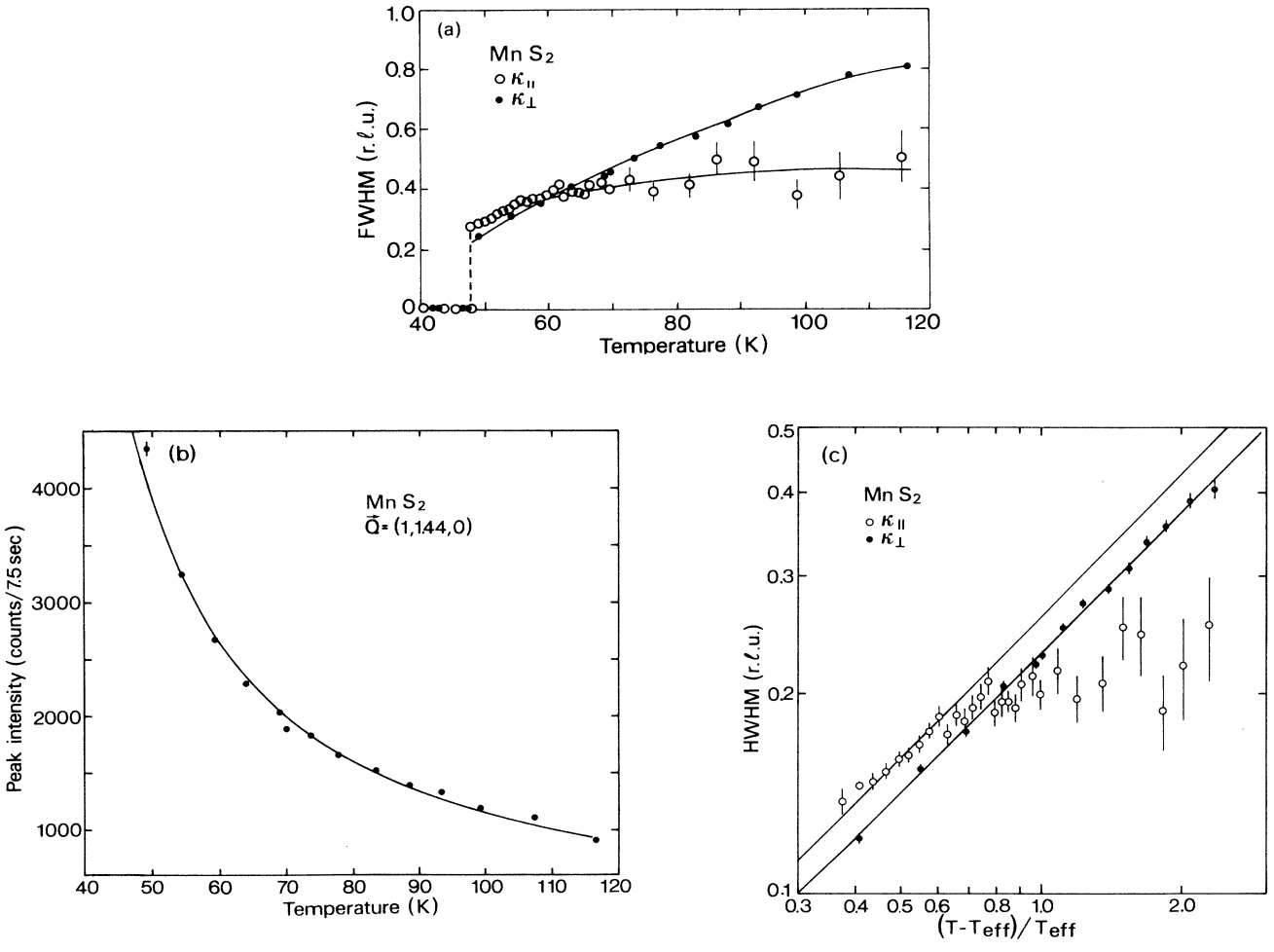

FIG. 7. Temperature variation of (a) the full width at half maximum (FWHM), which is proportional to the inverse correlation length, parallel and perpendicular to the modulation vector and (b) the peak intensity. (c) gives the log-log plot of the inverse correlation lengths vs reduced temperature. The straight line corresponds to the three-dimensional Heisenberg critical exponent $\nu=0.7020$. The effective Néel temperature obtained from the least-squares fit is $T_{\text{eff}}=35.0(5)$ K.

rately can be fitted to the three-dimensional Heisenberg exponent $\nu=0.7020$ very well by varying the effective Néel temperature T_{eff}. Figure 7(c) gives the log-log plot of the temperature variation of the perpendicular correlation length corresponding to the effective Néel temperature $T_{\text{eff}}=35.0(5)$ K. However, as is seen from the same figure, the parallel inverse correlation length does not fit very well to the above values of ν and T_N for temperatures higher than about 70 K. We have already mentioned that our determination of the parallel correlation length is not very accurate above 70 K due to the slopping background the origin of which is still to be investigated. The solid curve in Fig. 7(b) is the result of the least-squares fit of the peak intensity data using $T_{\text{eff}}=35$ K, which gave the critical exponent $\gamma=1.35$, a value close to the theoretical three-dimensional Heisenberg value $\gamma=1.375$.

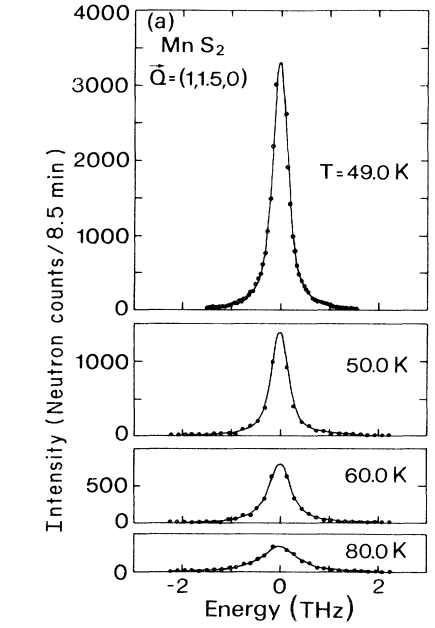

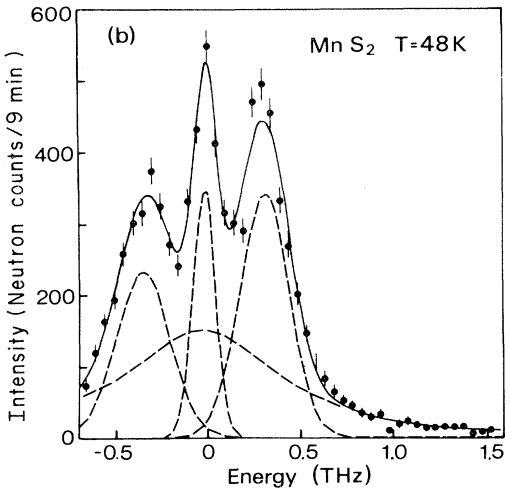

FIG. 8. (a) Quasielastic diffuse neutron magnetic scattering from MnS_2 in energy scans at several temperatures above T_N. The solid curves fitted to the data are of Lorentzian form convoluted with the Gaussian resolution function. (b) Energy scan just below T_N showing inelastic excitations (spin waves). The solid curve is the result of the least-squares fit of two Gaussians for the spin-wave peaks along with a Gaussian for the elastic peak and a Lorentzian describing the longitudinal fluctuations.

V. MAGNETIC DIFFUSE SCATTERING AS A FUNCTION OF E

We have investigated the magnetic diffuse scattering from MnS_2 as a function of the energy transfer at several positions in reciprocal space. Figure 8(a) shows the temperature dependence of such energy scans at $Q=(1,1.5,0)$. The solid curves are the results of least-squares fits of the data with Lorentzian curves convoluted with the Gaussian resolution curve obtained from the energy scan with vanadium. The full width at half maximum (FWHM) which is proportional to the inverse time correlation of the spin fluctuations is plotted as function of temperature in Fig. 9. The FWHM of the resolution is 0.19 THz. Figure 9 also shows the FWHM of the energy scans at $\mathbf{Q}=(1,1.44,0)$. From this figure we notice that the inverse time correlation is not very sensitive to a small change in Q ($\Delta Q_y=0.06$) close to the zone boundary and that data for $\mathbf{Q}=(1,1.5,0)$ and $\mathbf{Q}=(1,1.44,0)$ lie on a common curve. This is understandable because, even just above T_N, the inverse correlation length is large (the scattering is broad in Q) and we are still very far from critical behavior. The inverse time correlation of the spin fluctuations increases continuously with temperature from 0.16 THz just above T_N up to 2.9 THz at 150 K, the highest temperature at which the energy scan has been performed. As in the case of the spatial spin correlations, there is also no divergency of the spin correlations in time at the phase transition, which is consistent with its first-order nature. This is illustrated in Figs. 8(a) and 8(b), which show energy scans just above (49 K) and just below (48 K) $T_N=48.2$ K. While the frequency spectrum of the magnetization fluctuations is purely quasielastic above T_N, sharp inelastic excitations (spin waves) appear in the long-range-ordered phase. Note that, in the inves-

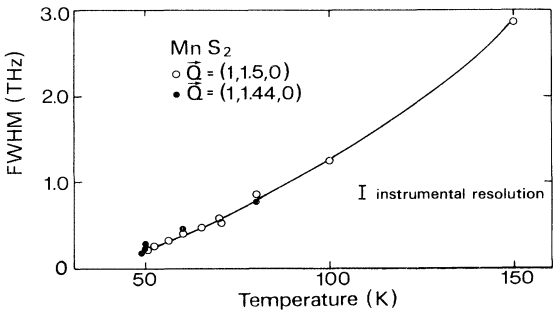

FIG. 9. Temperature variations of the full width at half maximum (FWHM) of the energy scans of MnS_2.

tigated temperature range above T_N and throughout the Brillouin zone, the energy width of the spin fluctuations stays always significantly smaller than the incident energy of $E=3.55$ THz. This justifies our integral measurements discussed in Sec. IV. The integrated intensity from our energy scans follows well the behavior of the peak intensity from the integral scans shown in Fig. 7(b).

VI. MEAN-FIELD CALCULATIONS OF THE MAGNETIC DIFFUSE NEUTRON SCATTERING ABOVE T_N

A. Magnetic diffuse neutron-scattering cross section

In order to obtain a deeper understanding of the paramagnetic magnetization fluctuations, we have performed model calculations of the magnetic diffuse neutron-scattering cross section. This cross section is directly proportional to the generalized wave-vector-dependent susceptibility tensor and thus measures the Fourier components of the microscopic magnetization fluctuations. In our case, we can assume the validity of the so-called "quasistatic approximation"[14] at all temperatures between T_N and 100 K, since the measured energy width of the magnetization fluctuations (<1 THz) always stays much smaller than the energy equivalent $k_B T$ of the corresponding temperature and also than the energy of the incident neutrons (3.5 THz). Thus, we can write the energy-integrated magnetic diffuse neutron-scattering cross section in the form[14]

$$\frac{d\sigma}{d\Omega}=N(\gamma r_0)^2|F(\mathbf{Q})|^2 e^{-2W}\frac{k_B T}{g^2\mu_B^2} \times \sum_{\alpha\beta}(\delta_{\alpha\beta}-\hat{Q}_\alpha\hat{Q}_\beta)\sum_{dd'}\chi_{dd'}^{\alpha\beta}(\mathbf{Q})e^{i\mathbf{Q}\cdot(\rho_d-\rho_{d'})} . \quad (1)$$

Here N denotes the number of unit cells, $\gamma r_0=0.539\times10^{-12}$ cm the coupling constant, $F(\mathbf{Q})$ the magnetic form factor for a single Mn^{2+} ion as a function of the scattering vector $\mathbf{Q}$, e^{-2W} the Debye-Waller factor, $\chi_{dd'}^{\alpha\beta}(\mathbf{Q})$ the tensor of the generalized susceptibility. The term $(\delta_{\alpha\beta}-\hat{Q}_\alpha\hat{Q}_\beta)$ accounts for the fact that only magnetic moment components perpendicular to the scattering vector contribute to the scattering process. The sum over d,d' runs over one unit cell and the indices d,d' label the magnetic ions within one cell at positions $\boldsymbol{\rho}_d,\boldsymbol{\rho}_{d'}$.

B. Model Hamiltonian

In the temperature range considered, MnS_2 behaves as a Mott insulator and we can attribute each Mn^{2+} ion a spin of fixed magnitude $S=\frac{5}{2}$ and an angular moment $L=0$. Since the free Mn^{2+} ion has a spherical symmetrical ground state, we neglect the single-ion anisotropy in the cubic crystalline field. Assuming that the Mn^{2+} spins are coupled via an isotropic exchange only, we then end up with a simple Heisenberg exchange Hamiltonian

$$\mathcal{H}=\sum_{ld,l'd'}J_{ld,l'd'}\mathbf{S}_{ld}\cdot\mathbf{S}_{l'd'} , \quad (2)$$

where $J_{ld,l'd'}$ is the exchange integral between a spin $\mathbf{S}_{ld}$ in the unit cell with label d and another spin $\mathbf{S}_{l'd'}$. For a Mott insulator, only short-range exchange interactions have to be considered. In our case, an inspection of the exchange paths lead to the conclusion that nearest-(J_1) and next-nearest-(J_2) neighbor interactions should be dominant. This is supported by calculations[15] that indicate that J_1 and J_2 are comparable and J_3 is only about 4% of these values.

C. Generalized susceptibility

The wave-vector-dependent susceptibility $\chi_{dd'}^{\alpha\beta}(\mathbf{Q})$ of (1) can be calculated for the model Hamiltonian (2) in the framework of molecular-field theory. While molecular-field theory is exact in the limit $T\to\infty$, it will give sufficiently good results for the magnetization fluctuations as long as short-range order (SRO) can be neglected.

According to de Gennes and Villain,[16] the mean-field expression for the wave-vector-dependent susceptibility in the paramagnetic state is given by

$$\chi_{dd'}^{\alpha\beta}(\mathbf{Q})=\delta_{\alpha\beta}g^2\mu_B^2[\underline{A}^{-1}(\mathbf{Q})]_{dd'} , \quad (3)$$

Evidently, the susceptibility is a scalar quantity in the paramagnetic state. The matrix $\underline{A}$ is given by

$$A_{dd'}(\mathbf{Q})=\frac{3k_B T}{S(S+1)}\delta_{dd'}-2J_{dd'}(\mathbf{Q}) \quad (4)$$

with $J_{dd'}(\mathbf{Q})$ as the Fourier transform of the exchange integrals. This form of χ is a generalization of the Curie-Weiss law $\chi=C/(T-\Theta)$. Equations (1)–(4) allow the calculation of the magnetic diffuse neutron-scattering cross section as a function of $\mathbf{Q}$ and T for given exchange parameters J_1, J_2, J_3, and J_4.

D. Comparison with experiment

At $T=65$ K we have performed linear scans in the (001) reciprocal-lattice plane. In order to correct for nuclear background scattering, the same scans were repeated at $T=200$ K. Figure 10(a) shows the distribution of the modulation of the magnetic diffuse intensity resulting from a difference (65−200 K) in form of a contour plot. Maxima are observed close to the points $(\frac{1}{2},1,0)$, $(\frac{3}{2},1,0)$, $(1,\frac{3}{2},0)$, etc., but already from this plot a shift of the centers to incommensurate values can be noticed.

We have performed the corresponding model calculations for various values of the exchange parameters, keeping the Néel temperature of the type-III ordering $[T_{N3}=\frac{2}{3}S(S+1)(-4J_1+2J_2)]$ constant at 48.2 K. This is, of course, not completely justified, as mean-field theory does not correctly reproduce the ordering temperatures and predicts a second-order phase transition in contrast to the observation.

On the other hand, mean-field theory should at least give qualitatively correct results at $T=65$ K, since the correlation length of about 5 Å indicates that the short-range order does not yet extend over large spin clusters (compare the distance of $R_1=4.3$ Å for nearest and $R_2=6.1$ Å for next-nearest neighbors). Figure 10(b) shows a model calculation corresponding to the same sit-

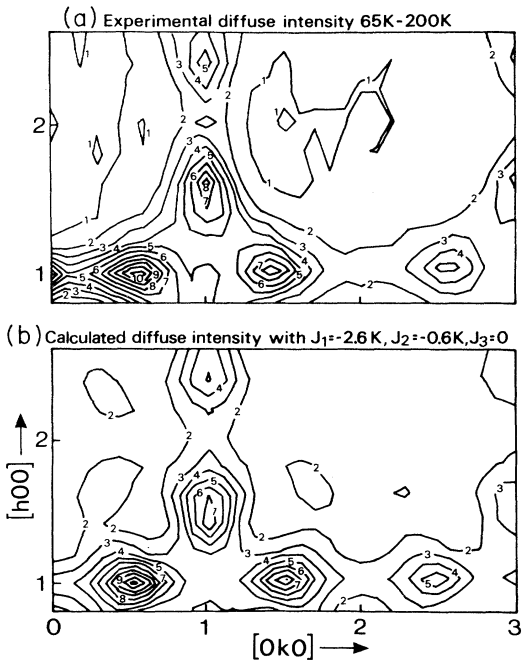

FIG. 10. (a) Contour plot of the magnetic diffuse scattering intensity in the (001) plane. To suppress nuclear background, the difference 65−200 K is plotted. Measurements were taken as 10 scans of each 31 points along the **b*** direction. Contour lines are equidistant (400 counts) between −200 and +3800 counts. (b) Calculated magnetic diffuse scattering cross section for the same reciprocal plane as in (a). Again, the difference between 65 and 200 K is plotted. A convolution with the resolution function was taken into account but is essentially negligible since the longest axes of the resolution ellipsoid corresponds to 0.11 r.l.u. For this calculation we have taken $J_1=-2.31$ K, $J_2=-0.50$ K, $J_3=0$. Contour lines are equidistant (1 b/sr) and lie between 0 and 13 b/sr.

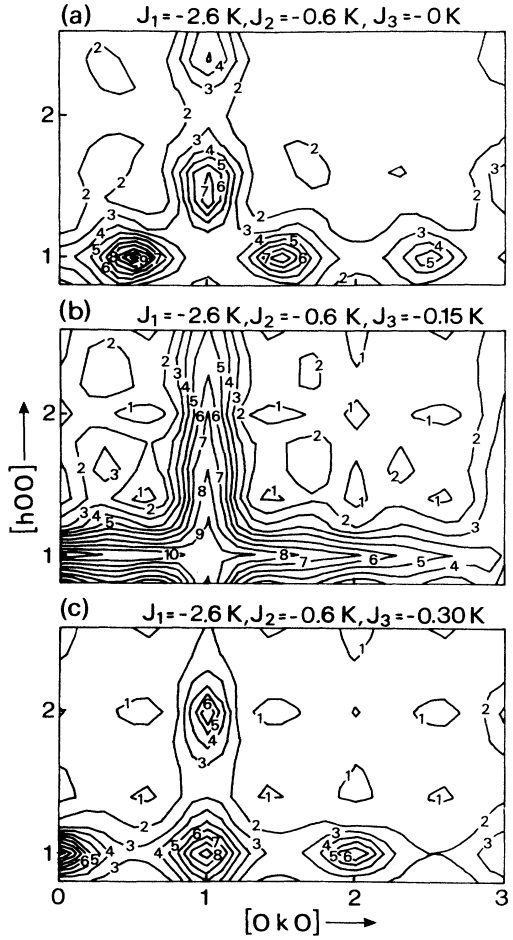

FIG. 11. Calculated difference between 65 and 200 K of the magnetic diffuse scattering cross section. The same reciprocal-lattice plane as in Fig. 10 is shown. J_1 and J_2 are the same for all three figures ($J_1=-2.60$ K, $J_2=-0.60$ K) while $J_3=0$ in (a), $J_3=-0.15$ K in (b), and $J_3=-0.30$ K in (c).

uation as in Fig. 10(a) for the values $J_1=-2.31$ K, $J_2=-0.50$ K, and $J_3=0$ of the exchange parameters. The convolution with the instrumental resolution function has been performed. The Mn^{2+} form factor has been included in the model calculations. Obviously, the main features of the observed intensity distribution can be reproduced. This includes the anisotropy of the width of the diffuse scattering in the $(h00)$ and $(0k0)$ directions. Although we start from a Hamiltonian that has full cubic symmetry, such an anisotropy is, of course, possible since the reciprocal-lattice point at which the diffuse scattering occurs has a lower point symmetry. The peak positions are found to be commensurate and the experimentally observed shift to the incommensurate position cannot be explained in this model. This will be discussed in detail in Sec. VII. It is important, however, to note that ratios of J_1/J_2 closer to one as suggested by calculations of the exchange parameters[15] are in clear disagreement with our observations. With such values for the exchange parameters, one would observe additional maxima in the magnetic diffuse scattering due to critical fluctuations of the type-II antiferromagnetic ordering.

In order to exemplify the influence of the exchange parameters for more distant neighbors, we have plotted in Fig. 11 the calculated intensity distributions corresponding to situations with three different values of the third-neighbor exchange J_3 ($J_3=0.00$, -0.15, and -0.30 K), keeping J_1 and J_2 fixed ($J_1=-2.60$ K, $J_2=-0.60$ K). Similar intensity distributions can be produced by small ferromagnetic exchange between fourth neighbors ($J_4>0$). As can be seen from the figure, drastic changes in the magnetic diffuse scattering cross section can be obtained by very small variations of these more distant exchange integrals. Even so, values of J_3 and J_4 are small as compared to J_1 and J_2, they can in no way be neglected for an understanding of the magnetic properties of a fcc antiferromagnet like MnS_2. While in the case of Fig. 11(a) ($J_3=0$) only fluctuations characteristic for the antiferromagnetic ordering of type III are observed, one finds spin correlations characteristic for the type-I structure for $J_3=-0.30$ K [Fig. 11(c)]. Figure 11(b) shows an intermediate situation with $J_3=-0.15$ K. For this particular set of exchange parameters, the mean-field ground-

state energy for the type-I and type-III antiferromagnetic structures are identical. Thus, we do not obtain peaks of diffuse scattering corresponding to one type of structure, but instead ridges of scattering connecting maxima for both types of structures.

The difference between the type-I and type-III structures can be understood in terms of a stacking sequence of the A and B antiferromagnetic layers shown in Fig. 2: The type-I structure is characterized by a sequence $ABABA\ldots$, the type-III structure by $AB\overline{AB}A\ldots$. In the situation of Fig. 11(b), both sequences become equally probable due to a degeneration in energy and thus we would expect a random sequence of AB and $\overline{AB}$ bilayers. For the paramagnetic short-range order, this would result in an intensity distribution as shown in Fig. 11(b).

VII. DISCUSSION

Mn^{2+} ions in MnS_2 form a face-centered-cubic (fcc) sublattice. The fcc lattice is inherently frustrated with regard to antiferromagnetic ordering and, therefore, exhibit many different types of antiferromagnetic phases. Nearest-neighbor Ising antiferromagnets on the fcc lattice have zero-temperature ground states with large degeneracies which are not just due the symmetry.[17,18] At any nonzero temperature, fluctuations break the degeneracies: entropy favors the ground state(s) about which the density of states of low-energy excitations is the greatest, producing a well-defined long-range order. Villain *et al.*[17] called this phenomenon "ordering due to disorder" and noted that both thermal and quenched disorders could induce long-range order. This idea has been extended to the Heisenberg fcc antiferromagnets with only isotropic exchange coupling which have also ground states with continuous degeneracies.[19] Thermal fluctuations do select special ground states, typically the collinear ones.

The spatial configuration of the magnetic moments of the type-III magnetic structure is specified by the wave vectors $\mathbf{k}_1=2\pi/a(\frac{1}{2},1,0)$ and $-\mathbf{k}_1$, $\mathbf{k}_2=2\pi/a(0,\frac{1}{2},1)$ and $-\mathbf{k}_2$, $\mathbf{k}_3=2\pi/a(1,0,\frac{1}{2})$ and $-\mathbf{k}_3$ where a is the lattice constant. The type-III antiferromagnetism is associated with magnetic Bragg reflections at positions $\mathbf{G}\pm\mathbf{k}_i$, where $\mathbf{G}$ is a reciprocal-lattice vector and $i=1,2,3$. Diffraction experiments cannot distinguish between a single-$\mathbf{k}$ multidomain structure and a multi-$\mathbf{k}$ single-domain structure in a cubic system without the application of magnetic field or uniaxial stress. In the case of MnS_2, we have, however, established in our recent neutron-diffraction experiment under magnetic field that the magnetic structure of MnS_2 is actually of the single-$\mathbf{k}$ type.[12] There exist two possible cases of single-$\mathbf{k}$ type-III antiferromagnetic structure. The first is collinear and corresponds to the single-spin-density wave (SSDW) while the second variety is called the helical spin-density wave (HSDW). In our recent polarized neutron-diffraction experiment[12] using the generalized polarization device CRYOPAD, we have established that the magnetic structure of MnS_2 is really a collinear SSDW type.

Taking only the nearest-neighbor and next-nearest-neighbor interactions J_1 and J_2 into account, the condition for the stability of the type-III magnetic structure on a fcc lattice is[20]

$$J_1/2<J_2<0\ .$$

On the basis of a localized effective electron model,[15] applying first-order exchange-perturbation theory, the calculated exchange parameters can be made to satisfy the above stability condition by a suitable variation of the parameters resulting type-III magnetic structure of MnS_2, but the difference in stability with type-III structure is only very slight. We have demonstrated in Sec. VI that, by choosing exchange parameters which satisfy the above inequality, the diffuse magnetic scattering from MnS_2 above T_N can be approximately reproduced by mean-field calculations. However, no variation of the exchange parameters could produce the observed deviation of the diffuse scattering maxima from the commensurate Bragg positions of the type-III magnetic structure. Taking the third-nearest-neighbor exchange interaction parameter J_3 into account does not improve the situation. The maximum positions of the diffuse scattering contours are highly sensitive to the sign and magnitude of J_3 shifting them from type-III to type-I and -II commensurate positions readily. However, no choice of J_1, J_2, and J_3 could reproduce the diffuse scattering maxima at the experimental incommensurate positions. It is also clear that the inclusion of a higher-order neighbor interaction parameter will not reproduce the incommensurate magnetic diffuse scattering maxima. The introduction of anisotropy term in the Hamiltonian can produce the maxima of diffuse scattering at incommensurate positions as has been demonstrated by Sinha *et al.*[6] in UAs. Mn^{2+} has a spherical $^6S_{5/2}$ ground state with zero orbital moment and therefore possesses no single-ion anisotropy. However, MnS_2 can have exchange anisotropy which can, in principle, also produce diffuse scattering maxima at incommensurate positions. It is to be noted that the crystal structure of MnS_2 belongs to the low-symmetry primitive cubic space group $Pa\bar{3}$ having no fourfold axes and mirror planes. The four S_2 dumbbells of the unit cell are directed along four different body diagonal directions $\langle 111\rangle$. It is therefore likely that MnS_2 has an anisotropic exchange interaction between the Mn^{2+} ions via different Mn^{2+}-$(S_2)^{2-}$$Mn^{2+}$ superexchange paths. In this case, exchange interaction parameters become tensors and the calculation of magnetic diffuse scattering involves too many free parameters and has therefore not been attempted. One can speculate that higher-order exchange interaction like four spin interaction terms might also lead to diffuse scattering maxima at incommensurate positions.

The first-order antiferromagnetic phase transition[2-4] of MnS_2 cannot be explained by symmetry arguments within the framework of Landau-Lifshitz theory. The temperature variation of the vector at which the diffuse scattering maximum is centered (Fig. 5) suggests that the antiferromagnetic phase transition in MnS_2 can perhaps be understood as a first-order lock-in transition from the incommensurate short-range order to the commensurate phase at T_N.

VIII. SUMMARY AND CONCLUSIONS

We have investigated the diffuse magnetic scattering in the frustrated antiferromagnet MnS_2 based on a fcc lattice above T_N. The diffuse scattering maxima are situated at incommensurate positions corresponding to a wave vector $=(1,k_y,0)$ and their positions are temperature dependent. The component k_y increases continuously with temperature from $k_y=0.40$ at $T=115$ K to $k_y=0.44$ at temperature just above T_N. At $T_N=48.2$ K, k_y jumps abruptly to the commensurate value $k_y=\frac{1}{2}$. To our knowledge such behavior has been observed for the first time in any magnetic system. This result suggests that the antiferromagnetic phase transition in MnS_2 can be understood as the first-order lock-in transition from the incommensurate short-range order to the long-range-ordered commensurate phase at T_N. Mean-field calculations of the diffuse magnetic scattering by taking into account nearest-neighbor and the next-nearest-neighbor exchange interaction parameters agree reasonably well with the experimental data, but such calculations fail to explain the centering of the diffuse scattering at incommensurate positions. The introduction of even a higher-order neighbor exchange interaction parameter does not improve the situation. The introduction of an anistropy term in the Hamiltonian is necessary in order to explain the centering of the diffuse scattering at incommensurate positions as have been shown by Sinha *et al.*[6] in the case of UAs. Mn^{2+} ions are in the spherically symmetric ${}^6S_{5/2}$ ground state with zero orbital moment and therefore possess no single-ion anisotropy. Introduction of anisotropic exchange interaction seems to be crucial for the explanation of the centering of the diffuse magnetic scattering maximum at incommensurate positions. Higher-order exchange interaction such as the four-spin interaction term in the Hamiltonian might also lead to the same result. Such calculations are rather involved and have not yet been attempted by us.

ACKNOWLEDGMENTS

We wish to thank Professor H. G. von Schnering for his encouragement and support, Dr. J. Rossat-Mignod for critical discussions, and R. Chagnon for his technical help. One of the authors (T.C.) wishes to thank Max-Planck-Gesellschaft for financial support.

[1]J. M. Hastings, N. Elliot, and L.-M. Corliss, Phys. Rev. **115**, 13 (1959).
[2]J. M. Hastings and L.-M. Corliss, Phys. Rev. B **14**, 1995 (1976).
[3]T. Chattopadhyay, H. G. von Schnering, and H. A. Graf, Solid State Commun. **50**, 865 (1984).
[4]E. F. Westrum, Jr. and F. Grenvold, J. Chem. Phys. **52**, 3870 (1970).
[5]J. Rossat-Mignod, in *Neutron Scattering in Condensed Matter*, edited by K. Skold and D. L. Price (Academic, New York, 1986).
[6]S. K. Shinha, G. H. Lander, S. M. Shapiro, and O. Vogt, Phys. Rev. B **23**, 4556 (1981).
[7]B. Hälg, A. Furrer, W. Hälg, and O. Vogt, J. Phys. C **14**, L961 (1981).
[8]J. Rossat-Mignod, P. Burlet, J. Villain, H. Bartholin, Wang Tcheng-Si, D. Florence, and O. Vogt, Phys. Rev. B **16**, 440 (1977).
[9]T. Chattopadhyay, P. Burlet, J. Rossat-Mignod, H. Bartholin, C. Vettier, and O. Vogt, J. Magn. Magn. Mater. **63&64**, 52 (1987).
[10]T. Chattopadhyay, P. Burlet, L. P. Regnault, and J. Rossat-
[11]F. Hulliger and E. Moser, J. Phys. Chem. Solids **26**, 429 (1965); G. Brostigen and A. Kjekshus, Acta Chem. Scand. **24**, 2983 (1970).
[12]T. Chattopadhyay, P. Burlet, and P. J. Brown, J. Phys. Condens. Matter **3**, 5555 (1991).
[13]T. Chattopadhyay, H. G. von Schnering, R. Stansfield, and G. J. McIntyre, Z. Kristallogr. (to be published).
[14]S. W. Lovesey, *Theory of Neutron Scattering from Condensed Matter* (Oxford University Press, Oxford, England, 1984), Vol. 2.
[15]G. van Kalkeren, R. Block, and L. Jansen, Physica B **85**, 259 (1977).
[16]P. G. de Gennes and J. Villain, J. Phys. Chem. Solids **13**, 10 (1960).
[17]J. Villain, R. Bidaux, J. P. Carton, and R. Conte, J. Phys. (Paris) **41**, 1263 (1980).
[18]N. D. MacKenzie and A. P. Young, J. Phys. C **14**, 3927 (1981).
[19]C. L. Henley, J. Appl. Phys. **61**, 3962 (1987).
[20]J. Villain, J. Phys. Chem. Solids **11**, 303 (1959).